Measurement of the spatial extent of inverse proximity in a Py/Nb/Py superconducting trilayer using low-energy muon-spin rotation

M. G. Flokstra,[1] S. J. Ray,[1] S. J. Lister,[1] J. Aarts,[2] H. Luetkens,[3] T. Prokscha,[3] A. Suter,[3] E. Morenzoni,[3] and S. L. Lee[1]

[1]*School of Physics and Astronomy, SUPA, University of St. Andrews, St. Andrews KY16 9SS, United Kingdom*

[2]*Leiden Institute of Physics, Leiden University, Niels Bohrweg 2, 2333 CA Leiden, Netherlands*

[3]*Labor für Myonspinspektroskopie, Paul Scherrer Institute, CH-5232 Villigen PSI, Switzerland*

(Received 13 December 2012; revised manuscript received 22 January 2014; published 19 February 2014)

Muon-spin rotation has been used to observe directly the spatial variation of the magnetic flux density near the ferromagnetic-superconducting interface in a permalloy-niobium trilayer. Above the superconducting transition temperature T_c the profile of the induced magnetic flux density within the niobium layer has been determined. Below T_c there is a significant reduction of the induced flux density, predominantly near the ferromagnetic-superconducting interfaces. We are uniquely able to determine the magnitude and spatial variation of this reduction in induced magnetization due to the presence of the Cooper pairs, yielding the magnitude and length scale associated with this phenomenon. Both are inconsistent with a simple Meissner screening and indicate the existence of another mechanism, the influence of which is localized within the vicinity of the ferromagnetic interface.

DOI: 10.1103/PhysRevB.89.054510 PACS number(s): 74.78.Fk, 74.45.+c, 75.70.Cn, 76.75.+i

I. INTRODUCTION

Conventional s-wave superconductivity is usually found to be incompatible with ferromagnetism since the exchange field in a ferromagnet typically leads to a breaking of the Cooper pairs in the superconducting state and hence to a suppression of the superconducting order [1]. A variety of novel ground states can, however, arise in artificially fabricated nanostructures where interfaces are created between superconducting (S) and ferromagnetic (F) regions. For the case of superconducting-normal interfaces it is well known that superconducting order can extend into the normal metal on a length scale of the order of the superconducting coherence length ξ_s [2], the so-called *proximity effect*. For the case of S/F interfaces a number of scenarios are possible. In $S/F/S$ trilayers the unusual Larkin-Ovchinnikov-Fulde-Ferrell (LOFF) state [3,4] has been observed within a thin F layer [5,6], where the exchange field of the ferromagnet induces a spatially varying phase in the superconducting order parameter. Recently, the existence of a novel long-range equal-spin-triplet superconducting state in F layers has been reported [7–10]. A key ingredient for the generation of equal-spin triplets is that the singlet Cooper pair needs to interact with some form of inhomogeneous/noncollinear magnetization [11].

In the vicinity of F/S interfaces related phenomena can occur that involve the modification of the superconducting state due to the presence of the ferromagnet, known as *inverse proximity effects*. One proposed mechanism involves the polarization of Cooper pairs leading to a net spin polarization within the superconducting layer of opposite sign to that within the ferromagnetic layer [12–14]. This typically is expected to occur within a coherence length of the interface. Observing such effects directly is problematic since the interesting states usually occur at buried interfaces and often over short length scales. In Ref. [13] measurements on V/PdFe and V/Ni heterostructures showed a distortion of the NMR spectra below T_c, which could be explained by ferromagnetism penetrating the superconductor. In Ref. [14] polar Kerr effect measurements on Pb/Ni and Al/CoPd bilayers displayed an angle shift for temperatures below T_c originating from the superconducting layer, implying an additional magnetization in that region. In neither of these experiments was spatial information provided other than the observed changes appear to originate from the superconducting layer, and at best both experiments average over the full depth of the thin superconducting layer. Direct observation of the spatial variation of this induced magnetism would provide a significant validation of theory and would provide information complementary to studies of the mechanisms of long-range triplets and related phenomena.

In this paper we present results of low-energy muon (LEM) measurements on a Py/Nb/Py superconducting trilayer which directly probe the *spatial variation* of the induced magnetization profile in the superconducting layer. Above T_c, in the normal state, we observe a magnetic proximity effect whereby a magnetization is measured within the Nb layer, extending up to a few nanometers, due to the presence of the neighboring ferromagnetic layers. Below T_c, in the superconducting state, there is a significant reduction of this induced magnetization, but localized to the vicinity of the F/S interfaces. While the *sign* of this modification is consistent with a model involving the effective polarization of Cooper pairs [11,15], the effect we observe decays within the Nb layer over a distance significantly *smaller* than ξ_s. While we show that this effect clearly cannot be attributed to conventional Meissner screening, the question remains whether it arises from polarization of Cooper pairs (a spin triplet effect) or from suppression of the exchange field near the interface by singlet Cooper pairs.

II. EXPERIMENTAL DETAILS

The measured sample is a 4×4 mosaic of Nb(2)/Py(20)/Nb(50)/Py(50)/Si thin films (layer thicknesses in nanometers) grown on 1×1 cm^2 square Si(100) substrates. They were prepared by dc magnetron sputtering in an ultrahigh vacuum chamber with a background pressure of 10^{-9} mbar and an Ar pressure of 4 μbar for Nb and 2.5 μbar

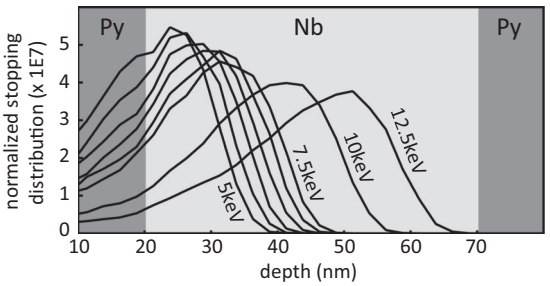

FIG. 1. Normalized muon stopping profiles for a Py(20)/Nb(50)/Py(20) trilayer (thickness in nm) for the measured muon energies 5, 5.5, 6, 6.5, 7, 7.5, 10, and 12.5 keV calculated using Monte Carlo simulations. Increasing the energy increases both the average implantation depth and the range of stopping distances.

for Py. During growth the substrate holders were equipped with a small magnet to determine the direction of easy axis for the Py layers, and the 2-nm Nb capping layer was added to prevent oxidation of the top Py layer. Py ($Fe_{20}Ni_{80}$) has a degree of spin polarization close to 45% and a Curie temperature around 900 K. The purity of the Nb target is 99.95% which yields a T_c of 9.1–9.2 K. The use of a large area mosaic ensured almost 100% coverage of the muon beam.

The muon is an unstable spin-$\frac{1}{2}$ lepton of charge $+e$ with a lifetime of $t_\mu = 2.197\ \mu$s. On decay it emits a positron at angle θ with respect to its momentary spin direction. The probability distribution for θ is given by $1 + (1/3)\cos\theta$. On implantation into a material the muon is rapidly thermalized, maintaining its initial spin polarization. The spin precesses around the local field with angular velocity that depends directly on the strength of the local flux density ($\omega = \gamma_\mu B$, where $\gamma_\mu = 851$ Mrad s^{-1} T^{-1} is the gyromagnetic ratio for the muon). In a muon-spin rotation (μSR) experiment the precession of spin-polarized muons can be monitored by the detection of the emitted positrons. A key feature of the unique low-energy muon facility is that the momentum of the muons can be reduced to a very low values [16]. This allows the implantation depth into the sample to be controlled on length scales compatible with thin-film structures (∼10 nm), in contrast to conventional μSR, where typical implantation depths are ∼100 μm.

Measurements were performed in a constant field of 9.7 mT, applied in the normal state with the field orientation within the plane of the film along the easy axis of the Py layers. This field is sufficient to saturate the Py layers and hence to minimize the influence of any stray fields due to magnetic domain formation. The muons were incident normal to the plane of the film and were spin-polarized in the plane of the film, perpendicular to their momentum direction. Two positron detectors were used, situated on the left and right of the sample, with the field lying in the vertical direction. Approximately 10 million detection events were recorded at each energy and temperature. The stopping profile for each energy is calculated using a well-proven Monte Carlo technique applied to the density profile of the sample (Fig. 1) [16]. Increasing the muon energy increases the average implantation depth of the muons but also increases the range of distances over which the muons come to rest. At the lowest energy (5 keV) the muons predominantly probe the F/S-interface region nearest the surface. By increasing the energy in increments of 0.5 up to 7.5 keV the profile is moved further into the Nb layer, and for the highest energy (12.5 keV) it covers the full depth of the Nb layer, weighted heavily by the center. By measuring the sample for all eight of these different stopping profiles (Fig. 1) we obtain spatial information.

III. RESULTS

The raw data obtained by the positron detectors as a function of time t and muon energy E is modeled by [16]

$$\begin{aligned} N_{\mathrm{L}}(t,E) &= N_0[1 + A(t,E)]e^{-t/t_\mu} + K_{\mathrm{L}}, \\ N_{\mathrm{R}}(t,E) &= \alpha N_0[1 - A(t,E)]e^{-t/t_\mu} + K_{\mathrm{R}}, \end{aligned} \tag{1}$$

where N is the number of measured positron counts, subscripts L, R denote left and right counting detectors, N_0 is the amplitude of the signal, K is the time-independent background contamination, and $\alpha \sim 1$ is the detector efficiency correction factor. $A(t,E)$ is the total asymmetry function and can be written as

$$A(t,E) = \frac{\alpha[N_{\mathrm{L}}(t,E) - K_{\mathrm{L}}] - [N_{\mathrm{R}}(t,E) - K_{\mathrm{R}}]}{\alpha[N_{\mathrm{L}}(t,E) - K_{\mathrm{L}}] + [N_{\mathrm{R}}(t,E) - K_{\mathrm{R}}]}. \tag{2}$$

It is the sum of the asymmetry contributions from each material layer. For our sample, we effectively sample the full muon beam so that the contribution to the asymmetry from muons hitting the Ag backing plate on which the sample is mounted is negligible, resulting in no undamped contribution to the asymmetry. In addition, the internal flux density of the Py layers is far above the maximum flux density that can be detected with the LEM apparatus. The only contribution to the detected asymmetry therefore comes from the Nb layer because all muons stopping in the Py layer are rapidly depolarized and do not contribute. The fraction of missing asymmetry at different energies is consistent with the fraction of muons stopping in the Py layer obtained from the Monte Carlo simulations.

In general the relaxing asymmetry can be modeled as

$$\begin{aligned} A(t,E) &= \int \mathcal{A}(t,E,x)G(t,E,x)dx, \\ \mathcal{A}(t,E,x) &= p(E,x)\mathcal{A}_0\cos[\gamma_\mu B(x)t + \phi_0(E)], \end{aligned} \tag{3}$$

where $p(E,x)$ is the muon stopping profile, G is the depolarization function ($G \leqslant 1$), $\phi_0(E)$ is the starting angle of the muon precession, and $\mathcal{A}_0$ is the maximum possible asymmetry that can be detected with the instrumental configuration (which is ∼27% using a Ag sample [17]). The integration runs over the full thickness of the Nb layer.

A common approach to the data analysis is to assume that for each implantation energy the signal can be modeled by a mean field [$\langle B(\bar{x})\rangle = B_0 = \text{const}$, $\bar{x}(E)$ is the mean stopping distance for energy E] and a simple depolarization function $G(t,E)$; for this system that data could be reasonably well described by $G(t,E) = e^{-\bar{\lambda}(E)t}$, with $\bar{\lambda}$ being the mean depolarization rate for energy E. Note that now the integration in Eq. (3) runs only over the stopping profile for that particular energy and simply gives the value of the initial asymmetry. While there is no longer a spatial coordinate involved, the dependence on muon energy is still a good

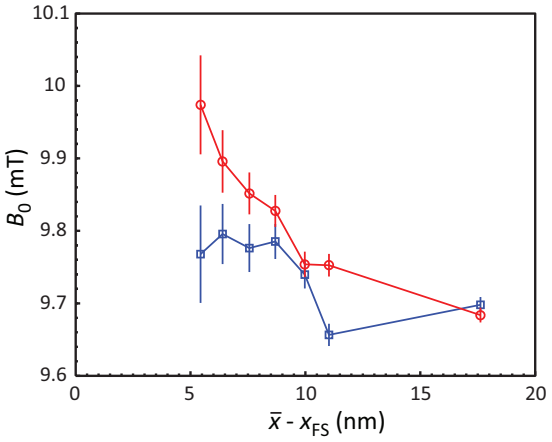

FIG. 2. (Color online) Obtained fit values for the mean flux density B_0 as a function of mean stopping distance inside the superconducting layer, $\bar{x}(E) - x_{FS}$, with x_{FS} being the position of the left-hand (topmost) Py/Nb interface (see Fig. 1) Circles: $T = 10$ K (Nb in the normal state); squares: $T = 4.3$ K (Nb in the superconducting state).

indicator of the spatial dependence since each muon energy effectively probes a different average depth $\bar{x}(E)$ within the sample. To fit the data to this model we use the iterative Levenberg-Marquardt algorithm. Fits were made for all data sets independently to obtain $B_0(E)$, and the result is presented in Fig. 2. A number of features are clearly apparent. First, for lower muon energies (towards the first F/S interface) the average field rises. In addition the associated uncertainty increases, consistent with a larger spread of fields around the mean field. Finally, the mean field in the superconducting state is below that of the normal state, especially for the lowest muon energies in the vicinity of the first F/S interface. In other words, towards the interface the internal field profile rises, but to a lesser extent for the case when the Nb layer is superconducting. Figure 3 shows the corresponding

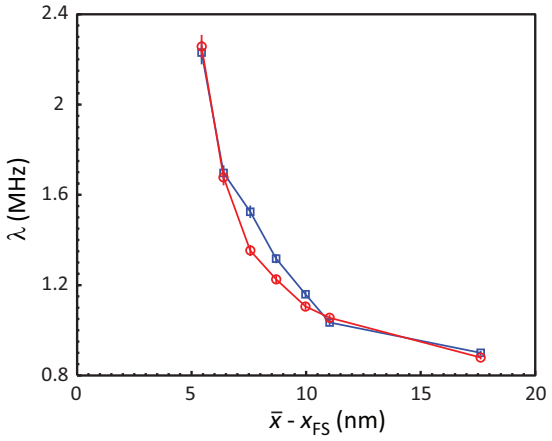

FIG. 3. (Color online) The value of the mean depolarization rate $\bar{\lambda}(\bar{x})$ obtained from fits to the data using a mean field for each muon implantation energy profile, corresponding to the mean flux density values in Fig. 2. Circles: $T = 10$ K (Nb in the normal state); squares: $T = 4.3$ K (Nb in the superconducting state).

decay parameter $\bar{\lambda}$ for which there is a very clear trend that implies an increasing depolarization rate towards the interface. The existence of any significant relaxation rate in the Nb is already interesting. A modest amount of damping in the normal state would be expected due to the randomly orientated nuclear dipole moments of Nb, which typically gives a contribution of the form $G(t) = \exp(-0.5\sigma_{Nuc}^2 t^2)$, but the more rapid damping $G(t,E)$ observed in these samples implies an additional source of flux density. Furthermore, the increasing value of $\bar{\lambda}$ for lower energies represents a further *broadening* of the flux density distribution about the average value, consistent with an induction profile $B(x)$ that rises towards the interface.

This magnetic proximity effect in the normal state of Nb could arise from a number of sources. At the applied fields used, the Py layers are well saturated with strong alignment of magnetic domains. Nonetheless, this broadening near the interface could arise from static dipolar fields penetrating the Nb layer from domain walls in the Py layer. It is also possible that in the normal state additional contributions to the muon depolarization may arise due to spin diffusion, although the spin diffusion length in Nb is known to be rather long, ~50 nm [18], so any associated flux density would be expected to vary only slowly over the width of the sample, leading to an average additional contribution. There might also be additional magnetization from rapidly oscillating Ruderman-Kittel-Kasuya-Yosida (RKKY)-type contributions to the spin polarization. Regardless of the source of this induced magnetization, it provides a useful background against which to measure the influence of the superconducting state below T_c.

While the simple mean-field fits presented in Fig. 2 provide a reasonable description of the data, significant improvement can be made using an alternative approach. In order to model the data better two features must be captured: as E is lowered and implantation moves towards the uppermost F/S interface there is both a rise of average induction and also an increased damping that cannot be well described by the exponential term alone. Rather than describe the sample as a series of mean-field steps, good fits for the $T > T_c$ data are obtained if one models the induction across the superconducting layer by

$$B^N(x) = B_0^N + B_1 f_1(x),$$
$$f_1(x) = \exp\left(\frac{-x + x_L}{\ell_1}\right) + \exp\left(\frac{x - x_R}{\ell_1}\right), \quad (4)$$

where x_L and x_R are the coordinates of the left and right interfaces, B_0^N is the background contribution due primarily to the external field, and ℓ_1 is the decay parameter. B_1 is the amplitude of the interface contribution, falling exponentially. At each energy E the flux density profile $B^N(x)$ is sampled with different weight at each value of x, determined by the stopping profile $p(E,x)$ and the calculated signal determined by the integral in Eq. (3). By including this flux density profile, as E is reduced, the average induction rises and also the damping increases since a greater *range* of flux density is also sampled near the F/S interface. The aim in fitting the data, which is done for *all energies simultaneously*, is to determine the form of $B^N(x)$ that is most consistent with the data across the full range of energies measured.

Below T_c we must also account for the *reduction* of the magnetization within the vicinity of the interface. This is

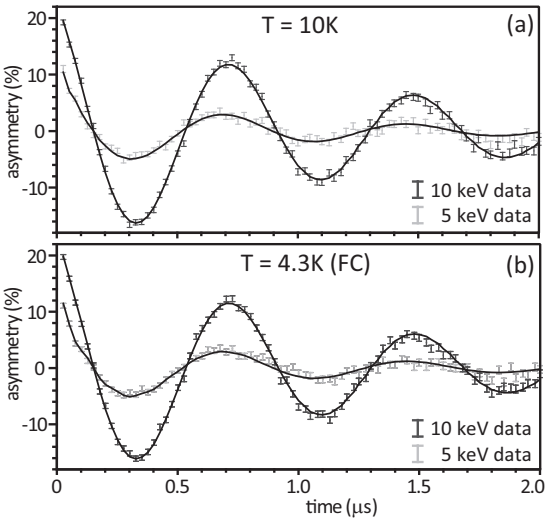

FIG. 4. Fits to the data taken in a field of 9.7 mT for energies of 5 and 10 keV (a) at 10 K and (b) after field-cooling (FC) to 4.3 K. The solid lines are fits using Eqs. (3) and (5) over *all energies*. Below T_c an additional term was included in Eq. (5) to account for the superconducting response (see text).

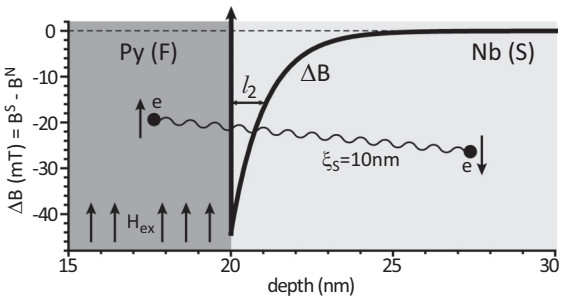

FIG. 5. The difference between $B(x)$ in the superconducting state and above T_c, $\Delta B(x) = B^S(x) - B^N(x)$. At the F/S interface the flux density in the superconducting state is considerably reduced compared to the normal state. The annotation is a schematic of Cooper pair polarization that might be expected due to an exchange field. The spatial extent of the observed effect $\sim \ell_2 = 1.1(1)$ nm is, however, significantly *smaller* than the coherence length $\xi_S \sim 10$ nm.

accounted for using a second exponential term with parameters B_2 and ℓ_2 that is added to a flux density profile similar to that for the $T > T_c$ data and that is able to account for any *change* in the field profile as the temperature is reduced.

$$B^S(x) = B_0^S + B_1 f_1(x) + B_2 f_2(x),$$
$$f_2(x) = \exp\left(\frac{-x + x_L}{\ell_2}\right) + \exp\left(\frac{x - x_R}{\ell_2}\right). \qquad (5)$$

The amplitude of this additional term is found to converge to zero when added to the fits to the data for $T > T_c$, and the requirement for this term is thus unique to the $T < T_c$ data. In the final analysis, all data sets are fitted simultaneously, including *all implantation energies* and data taken at *both temperatures*. In these fits the following constraints are applied: $\mathcal{A}_0(E)$ and $\phi_0(E)$ depend on energy only, $\lambda(T)$ and $B_0(T)$ have the freedom to depend on temperature, B_1 and ℓ_1 reflect the ferromagnetic properties of the sample and are tied together for all energies and temperatures, and B_2 and ℓ_2 are included only for $T < T_c$ in order to describe the *difference* in the magnetic profile below T_c. The additional exponential term involving B_2, ℓ_2, when combined with $B_0(T)$, has the freedom to account for a number of scenarios, including, for example, a simple Meissner screening with maximum flux expulsion in the center of the sample or, alternatively, a localized screening in the vicinity of the interfaces.

Two representative examples of spectra taken in the normal state at $T = 10$ K are presented in Fig. 4(a), one at 5 keV, weighted heavily to the region of the interface, and one at 10 keV, weighted more towards the center of the Nb layer. Both are clearly rather different from each other, both in terms of the measured asymmetry and the damping rate of the signal. Figrue 4(b) shows the corresponding data for $T = 4.3$ K. While the visual difference between curves at equal energy above and below T_c is very subtle, it is worth emphasizing that μSR is exquisitely sensitive to changes in flux density of well below 1 G. We also note the systematic shift of the mean field for all data above and below T_c (Fig. 2).

In Fig. 5 the main result of all fits is presented, namely, the *difference* between the induced flux density profile above and below T_c obtained from the global fits across all energies and temperatures (above and below T_c) simultaneously. Fits (examples given in Fig. 4) yield the following independent parameter values: $B_1 = 95(3)$ mT, $\ell_1 = 1.69(3)$ nm; for $T > T_c$, $\lambda = 0.75(1)$ MHz, $B_0 = 9.64(1)$ mT; and for $T < T_c$, $\lambda = 0.78(1)$ MHz, $B_0 = 9.61(1)$ mT, $B_2 = -44(3)$ mT, $\ell_2 = 1.1(1)$ nm. The mean value for $\mathcal{A}_0 = 26.5(0.6)\%$, which is consistent with that expected for the experimental arrangement.

IV. DISCUSSION

Above and below T_c the depolarization parameter λ shows no real difference within the uncertainties and represents a background level of depolarization within the Nb layer that is the same for all implantation energies. There is little difference in B_0 with temperature. The main difference with temperature thus comes from the additional exponential term with parameters B_2, ℓ_2, both the magnitude and sign of which are free to vary. The fit results show that in the center of the film, within the uncertainties there is little difference in the flux density between the normal and the superconducting states. That is, there is no significant Meissner screening. This is not unexpected given that the thickness of the Nb layer is of the order of the penetration depth and that the order parameter is suppressed due to the F layer, so that it is not possible for significant surface screening currents to develop. The main difference in the flux density profile with temperature, in fact, appears *near the F/S interface*, where the flux density in the superconducting state is noticeably reduced. We further note that in addition to having a different spatial profile, the magnitude of the observed effect in the vicinity of the interface ($\sim$44 mT) far exceeds that possible for Meissner screening, which even near the center of a bulk sample cannot exceed the applied field of $\sim$10 mT. This manifests in the mean-field fits of Fig. 2 as a relatively small shift because it originates from a region of the sample very close to the

F/S interface, $\sim\ell_2 = 1.1(1)$ nm, that contributes only a small weight to each spectrum due to the broad stopping profile of the muons (Fig. 1). Nonetheless, it is clearly measurable.

Such a reduction of flux density in the vicinity of the F/S interface cannot therefore be attributed to orbital screening currents, as in the Meissner state, which would lead to a maximum field expulsion in the center of the film, whereas there is effectively no difference in the center using either approach to fitting (Figs. 2 and 5). An alternative mechanism to consider is *spin screening* in the superconductor, which is predicted theoretically to be strongest at the interface. This mechanism for an "inverse proximity" effect may be viewed heuristically as arising due to one spin in a Cooper pair being aligned parallel to the exchange field of the ferromagnet in the vicinity of the interface (Fig. 5). The other spin is thus aligned antiparallel to the exchange field, leading to a net suppression of flux density inside the superconducting layer (Fig. 5). In order to consider the reduced flux density below T_c in terms of the polarization of Cooper pairs, we first estimate the density of pairs n_s from the London penetration depth $\lambda_L = e\sqrt{\frac{m}{n_s\mu_0}} \sim 32$ nm. If we then assign a Bohr magneton of moment to each electron of a polarized pair, the additional flux density at the interface $\sim$44 mT corresponds to a polarization of around 13% of the Cooper pairs in that region, which is physically reasonable. However, the natural length scale for the decay of such an effect is ξ_s, roughly the size of a Cooper pair (Fig. 5). In thin-film Nb $\xi_s \sim 10$ nm [19], which is *significantly longer* than the decay length $\ell_2 = 1.1$ nm observed in the superconducting state. Furthermore the magnetic length scale we observe in the normal state $\ell_1 = 1.69$ nm is itself much less than the quasiparticle spin diffusion length in Nb ($\sim$50 nm [18]), indicating the occurrence of additional magnetic proximity effects in the vicinity of the interface. In fact, the length of ℓ_1 is very similar to coherence length for a strong ferromagnet and thus consistent with the picture of induced magnetism in the Nb. The resulting local magnetic inhomogeneity may also need to be taken into account within a correct theoretical description of the superconducting response.

V. CONCLUSION

In conclusion, we have used low-energy μSR to observe directly the spatial variation of the flux density near the F/S interface. Above T_c the measurements are consistent with a flux density that falls exponentially from the interface into the S layer, and the short length scale suggests the origin is directly induced ferromagnetism in the S layer due to the exchange field in the F layer. Below T_c there is reduction of this interfacial magnetism, most pronounced near the F/S interface and negligible towards the center of the film, as would be expected from model calculations of the inverse proximity effect but over a length scale that would seem incompatible with this mechanism. The determination of the length scale of this reduction of magnetization via μSR is to date unique among measurement techniques that attempt to probe inverse proximity effects. The fact that no interfacial screening is observed on the scale of the superconducting coherence length is itself a challenge to theory and in contradiction to the interpretation of previous measurements, made in similar systems, that lacked spatial sensitivity. The results should provide a stimulus to theoretical models that consider these types of interactions and provide additional context in which to consider other experimental results on this type of system.

ACKNOWLEDGMENTS

We acknowledge the financial support of the EPSRC (Grant No. EP/J01060X). All experiments were carried out courtesy of the Paul Scherrer Institute.

[1] A. I. Buzdin, Rev. Mod. Phys. **77**, 935 (2005).
[2] P. G. De Gennes, Rev. Mod. Phys. **36**, 225 (1964).
[3] A. I. Larkin and Yu. N. Ovchinnikov, Zh. Eksp. Teor. Fiz. **47**, 1136 (1964) [Sov. Phys. JETP **20**, 762 (1965)].
[4] P. Fulde and R. A. Ferrell, Phys. Rev. **135**, A550 (1964).
[5] T. Kontos, M. Aprili, J. Lesueur, F. Genêt, B. Stephanidis, and R. Boursier, Phys. Rev. Lett. **89**, 137007 (2002).
[6] V. V. Ryazanov, V. A. Oboznov, A. Yu. Rusanov, A. V. Veretennikov, A. A. Golubov, and J. Aarts, Phys. Rev. Lett. **86**, 2427 (2001).
[7] R. S. Keizer, S. T. B. Goennenwein, T. M. Klapwijk, G. Miao, G. Xiao, and A. Gupta, Nature (London) **439**, 825 (2006).
[8] J. W. A. Robinson, J. D. S. Witt, and M. G. Blamire, Science **329**, 59 (2010).
[9] D. Sprungmann, K. Westerholt, H. Zabel, M. Weides, and H. Kohlstedt, Phys. Rev. B **82**, 060505 (2010).
[10] T. S. Khaire, M. A. Khasawneh, W. P. Pratt, and N. O. Birge, Phys. Rev. Lett. **104**, 137002 (2010).
[11] F. S. Bergeret, A. F. Volkov, and K. B. Efetov, Rev. Mod. Phys. **77**, 1321 (2005).
[12] F. S. Bergeret, A. F. Volkov, and K. B. Efetov, Phys. Rev. B **69**, 174504 (2004).
[13] R. I. Salikhov, I. A. Garifullin, N. N. Garif'yanov, L. R. Tagirov, K. Theis-Bröhl, K. Westerholt, and H. Zabel, Phys. Rev. Lett. **102**, 087003 (2009).
[14] J. Xia, V. Shelukhin, M. Karpovski, A. Kapitulnik, and A. Palevski, Phys. Rev. Lett. **102**, 087004 (2009).
[15] T. Löfwander, T. Champel, J. Durst, and M. Eschrig, Phys. Rev. Lett. **95**, 187003 (2005).
[16] P. Bakule and E. Morenzoni, Contemp. Phys. **45**, 203 (2004).
[17] H. Luetkens, Ph.D. thesis, University of Braunschweig, 2004.
[18] J. Y. Gu, J. A. Caballero, R. D. Slater, R. Loloee, and W. P. Pratt, Phys. Rev. B **66**, 140507 (2002).
[19] A. Yu. Rusanov, M. Hesselberth, J. Aarts, and A. I. Buzdin, Phys. Rev. Lett. **93**, 057002 (2004).